Research in Astronomy and Astrophysics, 25:045009 (6pp), 2025 April

https://doi.org/10.1088/1674-4527/adc64f
CSTR: 32081.14.RAA.adc64f

Astrophysical Priors on the Properties of Observed Black Hole–Neutron Star Mergers

Ya-Wen Xue[1], Ying Qin[1], Liang Yuan[1], Wei-Hua Guo[2], Jun-Qian Li[1], Yu-Qing Zhang[1], Zi-Yuan Wang[1], and Dong-Hong Wu[1]
[1] Department of Physics, Anhui Normal University, Wuhu 241002, China; yingqin2013@hotmail.com
[2] Institute for Theoretical Physics and Cosmology, Zhejiang University of Technology, Hangzhou 310032, China
Received 2025 January 26; revised 2025 March 23; accepted 2025 March 26; published 2025 April 10

Abstract

In this work, we analyze black hole-neutron star (BHNS) events using an astrophysically-motivated prior to derive updated, more tightly constrained estimates for component masses, mass ratios, and effective inspiral spin. For most BHNS systems, the mean primary mass shifts to higher values, with significant cases such as GW190426 and GW200115, where the primary mass is entirely excluded from the lower-mass gap. While the primary mass of GW230529 remains within the gap, its mean value shifts slightly upward. In contrast, the secondary mass generally shifts toward the higher end of the mass spectrum. These changes highlight the substantial influence of prior choices-particularly the spin prior-on the inferred mass distributions. Additionally, for all BHNS events, the effective inspiral spin is tightly concentrated around zero, reinforcing the expectation of nearly nonspinning components in these systems. We also discuss the classical common-envelope formation scenario, which is widely considered the dominant channel for BHNS formation, where the BH formed from the more massive progenitor star is typically expected to have negligible spin.

Key words: gravitational waves – stars: black holes – stars: neutron

1. Introduction

Mergers of black hole–neutron star (BHNS) systems are prime targets for gravitational wave (GW) detection by Advanced LIGO (Aasi et al. 2015), Advanced Virgo (Acernese et al. 2015), and KAGRA (Somiya 2012; Aso et al. 2013) observatories. By the end of the third observing run, the LIGO-Virgo-KAGRA (LVK) Collaboration had detected several BHNS events, including GW190426 (Abbott et al. 2021c), GW190917 (Abbott et al. 2024), GW191219, GW200105, and GW200115 (Abbott et al. 2021a, 2023a; Nitz et al. 2023). At the beginning of the fourth observing run on 2023 May 29, the high-significance detection of GW230529 occurred at 18:15:00 UTC, detected by the LIGO Livingston observatory while the other detectors were offline or insufficiently sensitive (Abac et al. 2024). The primary component mass of GW230529 was inferred as $m_1 = 3.6^{+0.8}_{-1.2}\,M_\odot$ (90% confidence interval) under a high-spin secondary prior. Since the maximum NS mass is assumed to be 2.5, $M_\odot$ in this study, the system was classified as a BHNS merger, with the BH mass lying in the lower-mass gap (i.e., 2.5–5 $M_\odot$, see a recent review paper from Shao 2022). To date six BHNS candidates have been reported by the LVK Collaboration and their main properties are summarized in Table 1.

In previous studies, it was pointed out that the properties of binary BH systems (i.e., spin and component masses) depend on the choice of priors (i.e., Galaudage et al. 2021; Roulet et al. 2021; Vitale et al. 2022). In particular, some individual events were reanalyzed with different priors than the LVK default one. Assuming more massive BH with no spin, the less massive component of GW190412 was inferred to be fast spinning (Mandel & Fragos 2020). Similarly, Mandel & Smith (2021) suggested that a prior of nonspinning BH for GW200115 is more consistent with current astrophysical understanding. For GW190521, Fishbach & Holz (2020) pointed out that it likely straddles the pair-instability gap by reanalyzing its signal with a population-informed prior on less massive BH mass. Recently, Chattopadhyay et al. (2025) examined the effects of prior selection on the inferred properties of GW230529, finding that the inferred mass distribution is highly dependent upon the spin prior. The findings above confirm that the choice of a prior can play a critical role in inferring the properties of GW sources.

The classical Common Envelope (CE) scenario is the most widely accepted formation channel for the majority of BHNS binaries (e.g., Giacobbo & Mapelli 2018; Belczynski et al. 2020; Drozda et al. 2022; Shao & Li 2021; Broekgaarden et al. 2021; Zhu et al. 2024). In this framework, the immediate progenitor of a BHNS binary emerging from the CE phase is a close binary system comprising an NS or a BH and a helium star. If the first-formed compact object is a BH, its spin is expected to be negligible, as suggested by studies (Qin et al. 2018; Fuller & Ma 2019; Belczynski et al. 2020; Fuller & Lu 2022). This aligns with the near-zero spin distribution observed in BHNS candidate systems from the O3 GW catalog (Zhu et al. 2022), which may indicate that NSs in these systems

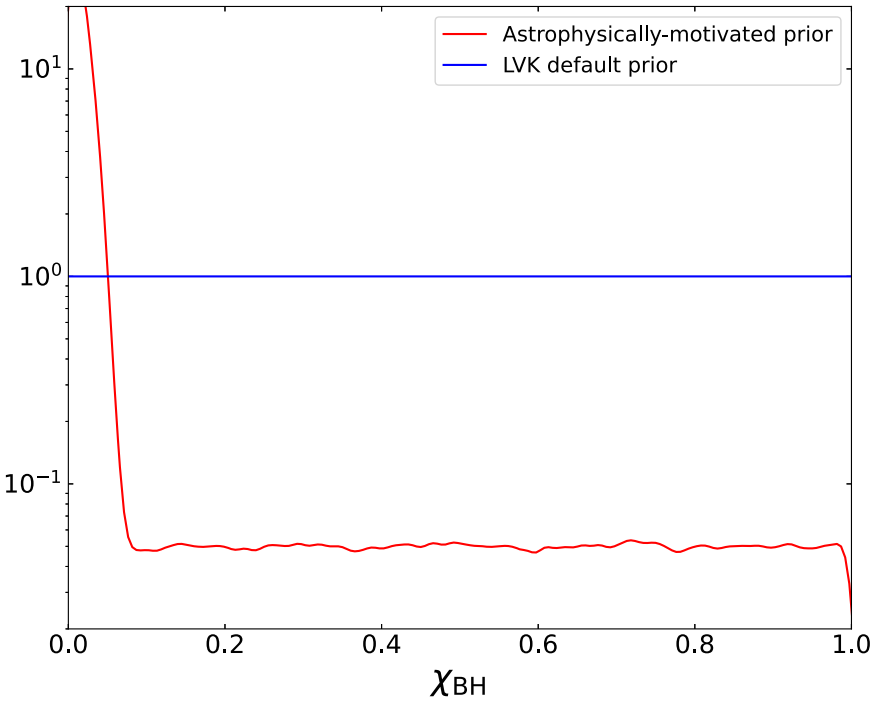

Figure 1. BH spin $\chi_{\rm BH}$ from an astrophysically-motivated prior (red) and the LVK default prior (blue).

Table 1
Main Properties of BHNS Candidates

Name	$m_1(M_\odot)$	$m_2(M_\odot)$	$\chi_{\rm eff}$	FA$R_{\rm min}$ (yr^{-1})	$p_{\rm astro}$	References
GW190426	$5.7^{+3.9}_{-2.3}$	$1.5^{+0.8}_{-0.5}$	$-0.03^{+0.32}_{-0.30}$	9.12×10^{-1}	0.14	(1)
GW190917	$9.3^{+3.4}_{-4.4}$	$2.1^{+1.5}_{-0.5}$	$-0.11^{+0.24}_{-0.49}$	6.56×10^{-1}	0.77	(1)
GW191219	$31.1^{+2.2}_{-2.8}$	$1.17^{+0.07}_{-0.09}$	$0.00^{+0.07}_{-0.09}$	4.0×10^{0}	0.82	(2)
GW200105	$8.9^{+1.1}_{-1.3}$	$1.9^{+0.2}_{-0.2}$	$-0.01^{+0.08}_{-0.12}$	2.04×10^{-1}	0.36	(3)
GW200115	$5.9^{+1.4}_{-2.1}$	$1.4^{+0.6}_{-0.2}$	$-0.14^{+0.08}_{-0.12}$	$\leqslant 10^{-5}$	>0.99	(3)
GW230529	$3.6^{+0.8}_{-1.2}$	$1.4^{+0.6}_{-0.2}$	$-0.10^{+0.12}_{-0.17}$	$\leqslant 10^{-3}$	/	(4)

References. (1) Abbott et al. (2023b); (2) Abbott et al. (2023a); (3) Abbott et al. (2021a, 2023b); (4) Abac et al. (2024).

are directly plunged into their companion BHs without significantly altering their spin. Conversely, for a subset of progenitor systems where the NS forms first, the helium star can be spun up via tidal interactions by the NS companion, potentially producing a BH with a high, aligned projected spin upon collapse (Qin et al. 2018; Hu et al. 2022). Given the currently observed low spins in BHNS populations, it is reasonable to conclude that the first scenario-where BHs form with negligible spin-dominates the contribution to most observed BHNS events.

In this work, we investigate the impact of astrophysical priors on the properties of BHNS populations and explore the implications for their origins. We begin by outlining the methodology in Section 2, followed by the presentation of our main results in Section 3. Finally, we summarize our key conclusions with some discussion in Section 4.

2. Methods

In our analysis, we utilize the posterior data derived from the low-spin prior template for GW191219, GW200105, GW200115, and GW230529. For GW190917 and GW190426, we adopt the IMRPhenomXPHM and PrecessingSpinIMRHM waveform models, respectively. Table 1 displays the posterior distributions of the component masses and the effective inspiral spins for all candidate BHNS events, obtained using the LVK default priors. With the assumption of a maximum NS mass of 2.5 $M_\odot$, GW190917 is classified as a BHNS event. Notably, GW190814 and GW200210

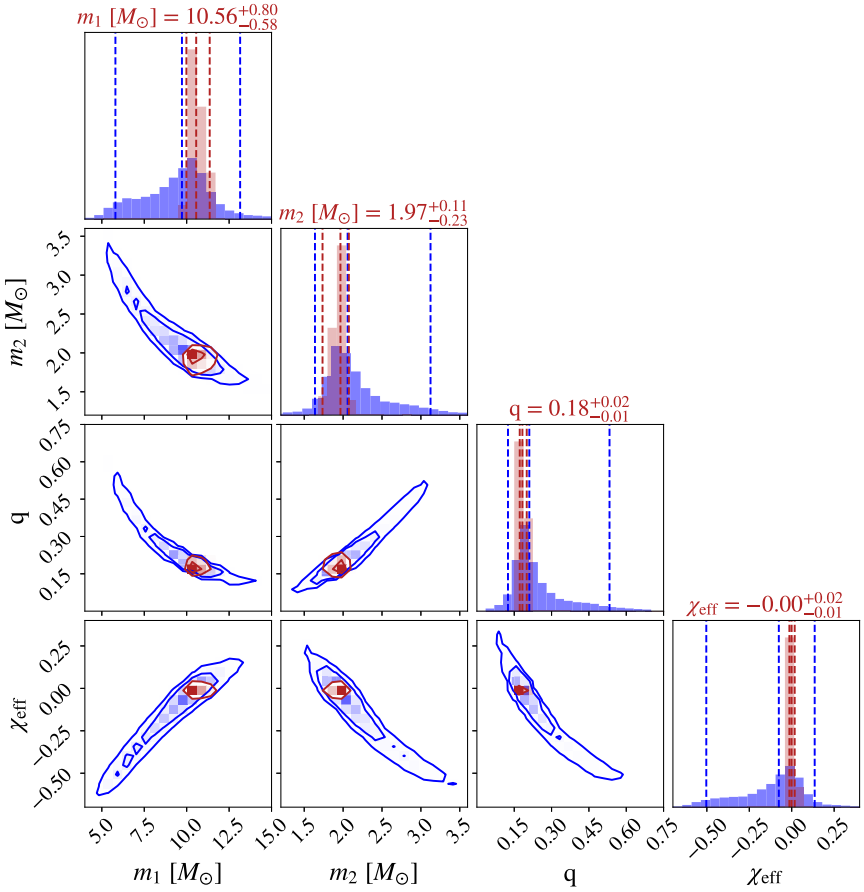

Figure 2. Corner plot (GW190917) showing the posterior distributions (Contours show 68% and 90% confidence intervals) for the primary mass m_1, secondary mass m_2, mass ratio q, and the effective inspiral spin $\chi_{\rm eff}$. The corresponding marginal posterior medians and three-sigma errors are also shown in dashed lines. Results are presented for the LVK default prior (blue) and the astrophysical prior (red). The remaining plots follow a similar trend and are therefore omitted for brevity.

are excluded from our analysis, as the inferred mass of the less massive component is higher than 2.5 $M_\odot$ (the maximum NS assumed in this study). The posterior data for these BHNS candidates were sourced from the Gravitational Wave Open Science Center (https://www.gw-openscience.org/eventapi/html/GWTC/; Abbott et al. 2021b).

It is widely accepted that the majority of BHNS binaries form through the classical isolated CE channel (Phinney 1991; Tutukov & Yungelson 1993; Hurley et al. 2002; Kalogera et al. 2007; Belczynski et al. 2016; Ablimit & Maeda 2018; Kruckow et al. 2018; Mapelli & Giacobbo 2018; Neijssel et al. 2019; Bavera et al. 2020; Belczynski et al. 2020; Drozda et al. 2022; Shao & Li 2021; Broekgaarden et al. 2021; Román-Garza et al. 2021; Hu et al. 2022; Mandel & Broekgaarden 2022; Xing et al. 2024). In this scenario, the more massive star evolves more rapidly than its companion, eventually expanding into a red supergiant after exhausting core hydrogen burning. During this phase, the outer hydrogen envelope is stripped through a combination of stellar winds and/or mass transfer to the companion. Consequently, the star loses the majority of its angular momentum, assuming efficient coupling between the stellar core and envelope (Spruit 2002). As a result, the first-born black hole, which forms prior to the CE phase, is expected to have a negligible spin (Qin et al. 2018; Fuller & Ma 2019; Belczynski et al. 2020). This expectation is consistent with the finding of negligible BH spin in BHNS candidates reported by Zhu et al. (2022). The secondary star could potentially be spun up into a fast-spinning, newly formed NS through efficient tidal interactions. However, it would quickly slow down due to magnetic braking. Consequently, NSs in BHNS mergers are generally expected to have low spins.

Using the methodology outlined in Mandel & Smith (2021), we adopt default priors for the component masses and assume independent spin magnitude distributions for the BH and NS. Figure 1 presents the two prior distributions of the BH spin magnitude, i.e., astrophysically-motivated prior and LVK default prior. These spin magnitudes follow truncated normal distributions centered at zero. The spin prior distributions are

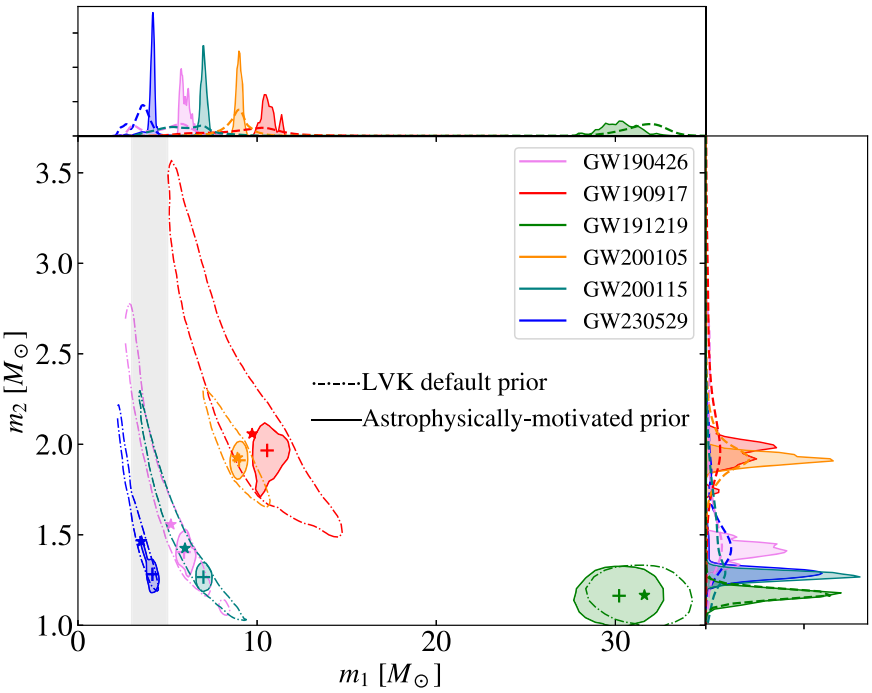

Figure 3. The posterior distributions of the component masses for the BHNS candidates are shown at the 90% confidence interval. The dashed line indicates results obtained using the LVK default prior, while the solid line represents results reweighted with an astrophysical prior. Star symbol: mean value for the LVK default prior, plus symbol: mean value for the astrophysically-motivated prior. The shaded region marks the mass range of 2.5–5.0 $M_\odot$.

defined as:

$$\begin{aligned}\pi_{\rm astro}(\chi_{\rm BH},\chi_{\rm NS}) = 0.95[&\mathcal{N}(\chi_{\rm BH};\mu=0,\bar{\sigma}=1.67\times10^{-2})\\ &\times\mathcal{N}(\chi_{\rm NS};\mu=0,\bar{\sigma}=1.67\times10^{-2})]\\ &+0.05\pi_{\rm LVK}(\chi_{\rm BH},\chi_{\rm NS}),\end{aligned} \tag{1}$$

where $\mathcal{N}$ denotes the normal distribution truncated to the interval [0, 1]. $\pi_{\rm LVK}(\chi_{\rm BH})$ and $\pi_{\rm LVK}(\chi_{\rm NS})$ represent the uniform distribution from 0 to 0.99. The parameter μ is the mean value, $\bar{\sigma} = 1.67 \times 10^{-2}$ is selected to ensure that each spin distribution has a standard deviation of approximately $\sigma_\chi = 0.01$.

To calculate the updated posteriors on BH mass m_1 and NS mass m_2, and $\chi_{\rm eff}$ under the astrophysical prior, we reweight the LVK posterior samples using:

$$w_{\rm i} = \frac{\pi_{\rm astro}(\chi_{\rm BH},\chi_{\rm NS})}{\pi_{\rm LVK}(\chi_{\rm BH},\chi_{\rm NS})}, \tag{2}$$

where $\pi_{\rm astro}$ and $\pi_{\rm LVK}$ represent the probability density of astrophysical prior and the default LVK prior used for each event's parameter estimation, respectively.

3. Results

With our target sample of BHNS events, we instead adopt the astrophysically-motivated prior to infer their properties, i.e., component masses, mass ratio, and effective inspiral spin. As an example, we first present the results for GW190917 in Figure 2. We note that the newly inferred primary mass $m_1 = 10.56^{+0.80}_{-0.58} M_\odot$ with the LVK default prior, while the secondary mass $m_2 = 1.97^{+0.11}_{-0.23} M_\odot$ is smaller compared to the LVK default prior. This updated result indicates a shift in the mass ratio ($q = m_2/m_1$) to a lower value. Notably, the updated parameters exhibit a narrower distribution, resulting in tighter constraints. Additionally, the effective inspiral spin is sharply concentrated around zero, suggesting that both components have nearly zero spins.

Figure 3 presents the newly inferred component masses for all BHNS events, analyzed using two distinct priors. For most BHNS events, the posterior distributions are more tightly constrained when employing the astrophysically-motivated prior. Notably, GW191219, the most asymmetric event, is inferred to have a primary mass of $30.21^{+1.70}_{-1.58} M_\odot$, which is slightly lower than the estimate obtained with the LVK default prior. Since the marginalized posteriors of individual parameters are correlated, our choice of prior not only affects the target parameter but also updates the posteriors of other correlated parameters (Vitale et al. 2017). This newly derived tighter constraint on the posterior shifts the mass ratio to higher values, leading to a lower primary mass. Furthermore, GW230529, recently reported at the start of the fourth observing run, is found to have a primary mass of

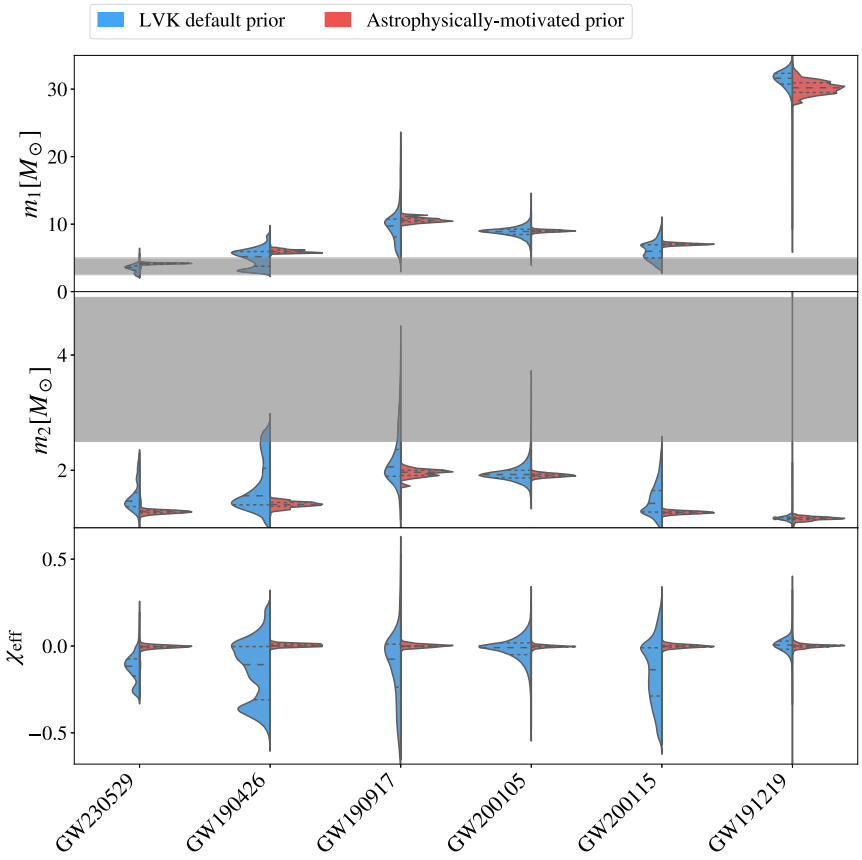

Figure 4. Violin plot showing marginal posterior distributions of primary mass m_1 (upper panel), and secondary mass m_2 (middle panel), and the effective inspiral spin $\chi_{\rm eff}$ inferred with LVK default prior (blue) and the astrophysically-motivated prior (red). The corresponding marginal posterior medians and one-sigma errors are also shown in dashed lines.

$4.16^{+0.15}_{-0.72} M_\odot$, placing it within the so-called lower-mass gap. This result aligns with previous findings, which indicate that the choice of spin prior significantly influences the inferred mass distributions (Chattopadhyay et al. 2025).

Figure 4 compares the component masses and effective inspiral spin using two distinct priors. For several BHNS events, particularly GW190426 and GW200115, the primary mass shows posterior samples partially falling within the lower-mass gap when analyzed with the default prior. In contrast, the astrophysically-motivated prior yields tighter constraints on the primary mass, with no samples lying in the lower-mass gap. Similarly, the secondary mass is more precisely constrained under the astrophysically-motivated prior, with its mean value shifting toward the lower end of the mass spectrum.

Additionally, the effective inspiral spin is tightly constrained around zero, implying that both the BH and NS exhibit negligible spins. This result supports the conclusion that a nonspinning binary scenario aligns better with current astrophysical expectations.

4. Conclusions and Discussion

In this work, we analyze BHNS events using an astrophysically-motivated prior, which provides updated and more tightly constrained estimates for component masses, mass ratios, and effective inspiral spin. For most BHNS systems, the mean primary mass shifts to higher values. Specifically, for GW190426 and GW200115, the posterior samples are fully excluded from the so-called lower-mass gap. While the primary mass of GW230529 still falls within the gap, its mean value shifts slightly toward higher values. Conversely, the secondary mass tends to shift toward the higher end of the mass spectrum. These shifts highlight the significant impact that the choice of prior, particularly the spin prior, has on the inferred mass distributions. Additionally, for all BHNS events, the effective inspiral spin is tightly concentrated around zero, reinforcing the preference for nearly nonspinning components in these systems.

It is widely accepted that the classical CE formation scenario is the dominant channel contributing to the BHNS population. In this scenario, the BH formed from the more massive progenitor star is generally expected to have negligible spin.

Acknowledgments

Y.W.X. acknowledges the support of the undergraduate Innovation and Entrepreneurship Training Program (No. S202410370441) and the Undergraduate Outstanding Thesis Cultivation Program (No. pyjh2024291). Y.Q. acknowledges support from Anhui Provincial Natural Science Foundation (grant No. 2308085MA29). This work is supported by the National Natural Science Foundation of China (grant Nos. 12473036 and 12103003). This work was partially supported by Jiangxi Provincial Natural Science Foundation (grant Nos. 20242BAB26012 and 20224ACB211001). All figures are made with the free Python module Matplotlib (Hunter 2007).

References

Aasi, J., Abbott, B. P., Abbott, R., et al. 2015, CQGra, 32, 074001
Abac, A. G., Abbott, R., Abouelfettouh, I., et al. 2024, ApJL, 970, L34
Abbott, R., Abbott, T. D., Abraham, S., et al. 2021a, ApJL, 915, L5
Abbott, R., Abbott, T. D., Abraham, S., et al. 2021b, SoftX, 13, 100658
Abbott, R., Abbott, T. D., Abraham, S., et al. 2021c, PhRvX, 11, 021053
Abbott, R., Abbott, T. D., Acernese, F., et al. 2023a, PhRvX, 13, 041039
Abbott, R., Abbott, T. D., Acernese, F., et al. 2023b, PhRvX, 13, 011048
Abbott, R., Abbott, T. D., Acernese, F., et al. 2024, PhRvD, 109, 022001
Ablimit, I., & Maeda, K. 2018, ApJ, 866, 151
Acernese, F., Agathos, M., Agatsuma, K., et al. 2015, CQGra, 32, 024001
Aso, Y., Michimura, Y., Somiya, K., et al. 2013, PhRvD, 88, 043007
Bavera, S. S., Fragos, T., Qin, Y., et al. 2020, A&A, 635, A97
Belczynski, K., Klencki, J., Fields, C. E., et al. 2020, A&A, 636, A104
Belczynski, K., Repetto, S., Holz, D. E., et al. 2016, ApJ, 819, 108
Broekgaarden, F. S., Berger, E., Neijssel, C. J., et al. 2021, MNRAS, 508, 5028
Chattopadhyay, D., Al-Shammari, S., Antonini, F., et al. 2025, MNRAS, 536, L19
Drozda, P., Belczynski, K., O'Shaughnessy, R., Bulik, T., & Fryer, C. L. 2022, A&A, 667, A126
Fishbach, M., & Holz, D. E. 2020, ApJL, 904, L26
Fuller, J., & Lu, W. 2022, MNRAS, 511, 3951
Fuller, J., & Ma, L. 2019, ApJL, 881, L1
Galaudage, S., Talbot, C., Nagar, T., et al. 2021, ApJL, 921, L15
Giacobbo, N., & Mapelli, M. 2018, MNRAS, 480, 2011
Hu, R.-C., Zhu, J.-P., Qin, Y., et al. 2022, ApJ, 928, 163
Hunter, J. D. 2007, CSE, 9, 90
Hurley, J. R., Tout, C. A., & Pols, O. R. 2002, MNRAS, 329, 897
Kalogera, V., Belczynski, K., Kim, C., O'Shaughnessy, R., & Willems, B. 2007, PhR, 442, 75
Kruckow, M. U., Tauris, T. M., Langer, N., Kramer, M., & Izzard, R. G. 2018, MNRAS, 481, 1908
Mandel, I., & Broekgaarden, F. S. 2022, LRR, 25, 1
Mandel, I., & Fragos, T. 2020, ApJL, 895, L28
Mandel, I., & Smith, R. J. E. 2021, ApJL, 922, L14
Mapelli, M., & Giacobbo, N. 2018, MNRAS, 479, 4391
Neijssel, C. J., Vigna-Gómez, A., Stevenson, S., et al. 2019, MNRAS, 490, 3740
Nitz, A. H., Kumar, S., Wang, Y.-F., et al. 2023, ApJ, 946, 59
Phinney, E. S. 1991, ApJL, 380, L17
Qin, Y., Fragos, T., Meynet, G., et al. 2018, A&A, 616, A28
Román-Garza, J., Bavera, S. S., Fragos, T., et al. 2021, ApJL, 912, L23
Roulet, J., Chia, H. S., Olsen, S., et al. 2021, PhRvD, 104, 083010
Shao, Y. 2022, RAA, 22, 122002
Shao, Y., & Li, X.-D. 2021, ApJ, 920, 81
Somiya, K. 2012, CQGra, 29, 124007
Spruit, H. C. 2002, A&A, 381, 923
Tutukov, A. V., & Yungelson, L. R. 1993, MNRAS, 260, 675
Vitale, S., Biscoveanu, S., & Talbot, C. 2022, A&A, 668, L2
Vitale, S., Gerosa, D., Haster, C.-J., Chatziioannou, K., & Zimmerman, A. 2017, PhRvL, 119, 251103
Xing, Z., Bavera, S. S., Fragos, T., et al. 2024, A&A, 683, A144
Zhu, J.-P., Hu, R.-C., Kang, Y., et al. 2024, ApJ, 974, 211
Zhu, J.-P., Wu, S., Qin, Y., et al. 2022, ApJ, 928, 167